Degradation by photo-Fenton process using Fe-clay as heterogeneous catalyst under sunlight and microwave irradiation

Amel Lounnas [a,*], Abdelhak Moumen [a,b], Emna Zouaoui [a], Youghourta Belhocine [a], Chafia Sobhi [b], Seyfeddine Rahali [c], Najoua Sbei [d,*]

[a] Laboratory of Catalysis, Bioprocess and Environment, Department of Process Engineering, Faculty of Technology, 20 August 1955 University of Skikda, P.O. Box 26, El Hadaik Road, 21000 Skikda, Algeria

[b] Department of Petrochemical, Faculty of Technology, 20 August 1955 University of Skikda, P.O. Box 26, El Hadaik Road, 21000 Skikda, Algeria

[c] Department of Chemistry, College of Science, Qassim University, Buraydah, Saudi Arabia

[d] Institute of Nanotechnology, Karlsruhe Institute of Technology, Eggenstein-Leopoldshafen, 76344 Karlsruhe, Germany

Keywords:
Clay
Methylene blue dye
Catalysts
Impregnation
Photo-Fenton reaction

A B S T R A C T

This study presents a newly developed, highly efficient heterogeneous iron-based catalyst (Fe-CY), supported on treated bentonite clay (CY), designed for the degradation of methylene blue (MB) dye. The bentonite clay underwent a two-stage treatment involving physical and chemical processes to produce the designated treated clay (CY), which served as the support material for Fe-CY catalyst preparation using the wet impregnation technique. Subsequently, the performance of the resulting catalyst was assessed in a photo-Fenton reaction aimed at degrading MB dye under both solar and microwave irradiation conditions. To determine the optimal decolorization conditions, several variables, including catalyst dosage, H_2O_2 quantity, pH, and initial MB concentration in the reaction system, were systematically investigated. Miscellaneous characterization techniques were employed to assess the support, and prepared catalyst. X-ray diffraction (XRD) was used to determine crystallinity, scanning electron microscopy (SEM) to analyze morphological structure, Fourier-transform infrared spectroscopy (FTIR) to identify surface functional groups, energy dispersive X-ray (EDX) analysis for the purpose of elemental analysis, and Brunauer-Emmett-Teller (BET) for analyzing the textural properties. The experimental findings highlight the remarkable effectiveness of the catalyst in degrading methylene blue (MB). Upon exposure to sunlight and microwave irradiation, the catalyst achieved substantial MB color removal rates of 99.5% and 95.5% within 180 and 8 min, respectively. Moreover, the stability of the catalyst was evaluated across three consecutive cycles, revealing a sustained removal efficiency of 83.05%. Finally, a comprehensive investigation into the mechanism behind methylene blue (MB) removal was conducted, revealing insights into the unique catalytic properties of the Fe-clay catalyst.

1. Introduction

The release of polluted industrial wastewater into natural ecosystems represents a serious issue for public health and environment, given its detrimental impacts. Industrial effluents are laden with harmful gases, heavy metals ions and a wide variety of toxic organic and inorganic compounds, including dyes [1]. For decades, researchers have deployed enormous efforts to eliminate dyes [2–4] by using and developing various techniques and materials [5–10]. The widespread application of dyes in diverse industries, such as textiles, paints, carpets, and printing, significantly contribute to environmental pollution issues [11]. Addressing the degradation or elimination of dyes poses a challenge, as achieving this goal without causing environmental issues is often complex due to the use of diverse chemical methods.

Among these dyes, the synthetic methylene blue (MB) stands out as frequently employed for industrial purposes, such as paper coloring, temporarily hair dyeing, cotton and wool dyeing, and paper stock coating. Additionally, MB finds applications as a histological dye, and an antimicrobial agent for minor wound treatment [12]. Considering the toxicity of synthetic dyes detected in surface waters, the removal and degradation of organic dyes have become a paramount concern [13]. Various physicochemical and biological techniques [14], such as

* Corresponding authors.
E-mail addresses: a.lounnas@univ-skikda.dz (A. Lounnas), najoua.sbei@kit.edu (N. Sbei).

coagulation [15], forward osmosis [16], adsorption [17], biosorption [18], membrane bioreactor [19], among others, were proposed for the treatment of wastewater containing dyes. However, these approaches frequently encounter difficulties due to high costs, environmental issues and diverse contaminant levels [20]. To overcome these limitations, recent efforts were focused on both cost-effective and environmentally friendly alternatives. Advanced oxidation processes (AOPs) are regarded as less polluting and more environmentally friendly, compared to traditional methods. They are recognized for their high efficiency in degrading a variety of organic compounds owing to their excellent oxidation capabilities [21,22].

Several techniques fall under the class of AOPs, including Fenton methods, photo-Fenton, wet oxidation, ozonation, electrochemical oxidation and photocatalysis [23,24]. The Fenton technique, in particular, stands out as one of the extensively studied methods due to its remarkable potentially useful, economical, and eco-friendly method of treating wastewater [25]. The Fenton reaction is key step within AOPs. In this process, hydrogen peroxide and Fe^{2+} salts act as primary reagents, generating hydroxyl radical (•OH) as the active intermediate responsible for eliminating pollutants from effluents [26–29].

Moreover, the homogeneous Fenton process demonstrates greater efficiency at a low pH (<3) by enhancing the reactivity and stability of H_2O_2, thus preventing the formation of iron sludge in water. However, the primary drawback of the homogeneous Fenton reaction is the difficulty associated with recovering Fe ions, thereby limiting its applicability [30,31]. To circumvent potential limitations, current research is directed towards more efficient techniques, with a particular focus on the photo-Fenton method. This approach employs a heterogeneous catalyst and uses various external energy sources, such as ultrasound, microwave (MW), UV radiation, visible light, UV lamps, and sunlight.

Among these alternatives, numerous studies demonstrated the advantages of using natural sunlight and microwave radiation. Natural sunlight is an abundant and readily available natural energy source that can reduce operational costs and minimize reliance on artificial radiation [32,33]. Meanwhile, microwave radiation can induce the formation of "hot spots" upon absorption by a catalyst, leading to increased radical generation and enhanced degradation of pollutants [34].

Heterogeneous catalysis plays a crucial role in certain AOPs [35], such as Fenton reaction and heterogeneous photo-Fenton reaction [36]. In this latter, Fe(III) is rapidly converted to Fe(II) upon exposure to light. These ions can then react with H_2O_2 to generate additional hydroxyl radicals, which oxidize organic pollutants such as dyes.

Numerous heterogeneous photo-Fenton catalysts, consisting of supported Fe oxides in materials such as clays, silica, carbon-based compounds, and metal oxides, were reported in the literature [37,38]. Solid supports have significant functions in sustaining metal oxide nanoparticles, as they offer an active surface location that contributes directly to the reactivity. Hence, many studies suggested clay minerals as catalyst supports due to their affordability, widespread availability and environmental friendliness. Furthermore, their structures govern essential physical and chemical properties, such as specific surface area, ion exchange capacity, and reactivity, including those related to metal and metal oxide nanoparticle catalysts [39,40]. The aim of this research is to develop a novel iron oxide-clay catalyst characterized by reliability, and efficacy in remediating water contaminated with organic dyes, such as methylene blue dye. We utilized and evaluated the potential of cost-effective, naturally occurring, processed local bentonite clay, treated as a support, to synthesize the Fe_2O_3-clay catalyst. This synthesis was carried out using the wet impregnation technique. This heterogeneous catalyst effectively eliminates MB dye from wastewater, using the photo-Fenton process under sunlight or microwave irradiation. Several operational factors, including catalyst dosage, H_2O_2 quantity, pH, and initial MB concentration were investigated. The catalyst was characterized using FTIR, XRD, BET, and SEM techniques.

2. Materials and methods

2.1. Materials

The bentonite clay employed in this study is yellow in color and originates from a deposit located in Eastern Algeria. All the chemicals used in this research are of analytical reagent grade. Sodium hydroxide (NaOH), sulfuric acid (H_2SO_4), hydrogen peroxide (H_2O_2 (30 %)), sodium chloride (NaCl), Ferric nitrate nonahydrate ($Fe(NO_3)_3{\cdot}9H2O$)) and methylene blue (MB) were supplied by Biochem Chemopharma Company. The molecular structure of MB is depicted in Fig. 1.

2.2. Materials and methods

2.2.1. Preparation of supported Fe-clay catalyst

The catalyst used in this study was prepared through the following steps:

Step 1: Support (clay) preparation

The bentonite clay, before being employed in the catalyst preparation for this study, underwent physicochemical treatments to remove soluble impurities and organic matter, according to the following protocol:

The natural clay was powdered and sieved, using a mill and a 150 μm sieve, respectively. The sample was subsequently rinsed with distilled water and H_2O_2 [42]. Then, the raw clay was mixed with a NaCl (1 M) solution and stirred for 12 h at room temperature. After settling, the supernatant was removed and this process was repeated several times. The resulting sample was then separated by centrifugation, filtered, and cleaned with distilled water until the chloride ions were eliminated (confirmed by adding a drop of 0.1 M $AgNO_3$). The purified sample was treated with H_2SO_4 (0.1 M) until saturation. After rinsing with distilled water, the treated sample was separated by filtration and dried at 105 °C [43]. Finally, the resulting sample is identified as CY.

Step 2: Impregnation of support with metal precursor solution

To achieve a uniform distribution of iron oxide on the clay surface, a wet impregnation process was employed in the synthesis of catalyst. Before impregnation, the bentonite clay support was prepared as outlined in the prior section. To achieve a solution with a Fe weight percentage of 5 %, a precise amount of $Fe(NO_3)_3{\cdot}9H_2O$ was dissolved in 100 ml of distilled water. Following this, 25 g of activated clay were gradually added to the mixture, which was then continuously stirred for 4 h at 60 °C. Subsequently, this solution was mixed with pre-moistened clay support in water. A gradual addition of 1 M NaOH solution was performed to attain pH of 10, ensuring complete precipitation of Fe_2O_3.

Step 3: Mixture treatments

The mixture was stirred vigorously, and subsequently, the excess

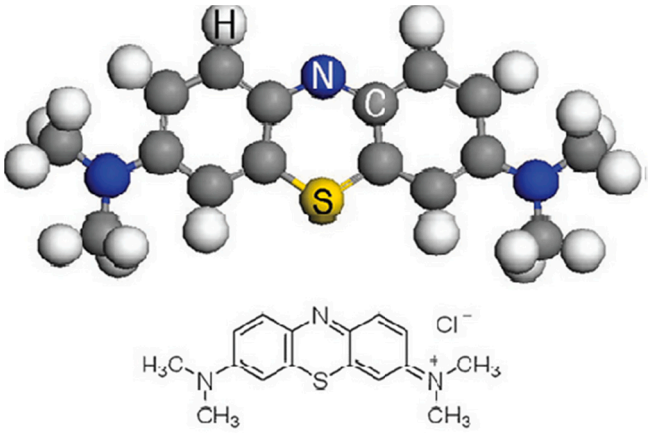

Fig. 1. Structure and model of MB dye molecule [41] (adapted with permission from the Royal Society of Chemistry, license ID 1079849–1).

water was evaporated by heating at 80–90 °C for 4 h, employing a sand bath. The resulting material underwent drying and calcination at 90 °C and 400 °C overnight and for 4 h, respectively.

The impregnation method resulted in a catalyst named Fe_2O_3-clay, designated as Fe-CY.

2.2.2. Apparatus

The crystalline structure of the samples was identified through X-ray diffraction (XRD) analysis using PANalytical X'Pert PRO diffractometer. The infrared spectra were recorded using a Thermo Scientific Nicolet iS10 Fourier transform spectrometer, within the spectral range of 4000 to 400 cm^{-1}. To measure MB concentration in the sample at 617 nm, a Shimadzu UV/Visible spectrophotometer (model UV1605, Japan) was employed.

Scanning electron microscopy analysis (SEM) was conducted, using a JEOL/JSM-6360LV microscope to identify the particle morphology of the samples. In addition, elemental analysis was conducted using an energy dispersive X-ray (EDX) technique with an EVO MA 25 microscope. The specific surface area was determined using the nitrogen adsorption–desorption method at 77 K, employing a surface area and porosity analyzer (Quantachrome Autosorb iQ Model 7 with AsiQWin Version 5.2).

2.2.3. Catalytic activity test

The catalytic efficiency of supported Fe-CY catalyst was assessed by degrading MB in aqueous solution under solar or microwave irradiation.

In each experiment, a predetermined amount of catalyst powder was added to previously prepared MB solution of 200 mL. The pH value was adjusted by adding NaOH or HCl prior to the introduction of H_2O_2. This step ensured uniform blending of catalyst with a solution and established adsorption/desorption equilibrium between the pollutant and the catalyst, before addition of H_2O_2.The mixture was stirred in dark for 5 min at 300 rpm. Then, a predetermined concentration of H_2O_2 was added to the mixture. The experiments were performed from May to July in Skikda, located in northeastern Algeria. During this time, the mixture was exposed to sunlight from 11:00 a.m. to 03:00p.m. Microwave-Fenton degradation experiments were conducted, using a power range of (200–500) W in a microwave oven. Periodically, 10 ml samples were taken, filtered, and analyzed with UV/visible spectrophotometer.

The discoloration amount of MB was calculated using the following equation:

$$C_{dis} = \frac{C_t}{C_0} \tag{1}$$

The experimental data are fitted by applying a pseudo-first order kinetics model defined by Mathews Weber equation:

$$\ln\frac{C_t}{C_0} = \quad kt \tag{2}$$

The half-life of the dye degradation

$$t_{\frac{1}{2}} = \frac{0.639}{k_{app}} \tag{3}$$

C_0 represents the initial concentration, while C_t denotes the concentration of MB solution (mg/l) at time t, k (min^{-1}) is the reaction rate constant and $t_{1/2}$ the half-life of dye degradation [44]. Additionally, various factors like catalyst dose, oxidant volume, pH, and concentration of dye were investigated.

2.2.4. Catalyst reusability test

To assess the stability of the catalysts, three sequential experiments were conducted using fresh dye solutions under optimal experimental conditions. After each run, the catalyst was filtered, cleansed with distilled water and acetone, and subsequently dried in a 110 °C oven overnight.

3. Results and discussion

3.1. Support and catalyst characterization

3.1.1. X-ray Diffraction (XRD)

The X-ray powder diffraction pattern for the treated clay, depicted in Fig. 2, exhibits main peaks observed at diffraction angles $2\theta = 20.08°$, 20.87°, 23.61°, and 26.65°, corresponding to d-spacing values of 4.44, 4.25, 3.76, and 3.35 Å, respectively. These peaks can be attributed to the presence of two phases: montmorillonite and quartz. Additionally, a peak at 27.42°, corresponding to a small quantity of (Fe_2O_3), was detected in the XRD pattern of the catalyst, confirming the presence of Fe formed on the surface of the catalyst, in agreement with observations of Mekatel et al. [45]. The absence of multiple peaks in the supported catalyst, indicating iron oxide, can be attributed to a well-distributed active phase on the support surface.

Furthermore, the low iron (Fe) content in the clay may contribute to this outcome, suggesting that the incorporation of iron did not significantly alter the structure of the clay. Consequently, the intensity of the peaks in the Fe-clay catalyst appears less pronounced and weaker compared to the clay peaks due to the presence of iron oxide. However, the prepared catalyst exhibits a notable degree of crystallinity, evident from the narrowness of the peaks.

3.1.2. Fourier transformed infrared spectroscopy (FTIR)

Fig. 3 shows the FTIR spectra of treated clay and Fe-CY catalyst in the range spanning from 500 to 4000 cm^{-1}. The peaks around 3600 cm^{-1} are attributed to hydroxyl groups. The band at 1670 cm^{-1} is assigned to the bending modes of water molecules. The broad bands observed at 1119 and 1032 cm^{-1} are associated with the stretching vibrations of Si-O in the treated clay [46].

In the DRX analysis, the absence of the Fe-O bond in the Fe-CY catalyst was clearly confirmed, as evidenced by the FTIR data. A distinctive band appears at approximately 560 cm^{-1}, indicating the presence of iron. However, the absence of this band in the FTIR spectrum suggests that the clay and iron might only have an electrostatic interaction instead of a covalent bond.

3.1.3. Scanning electron microscopy (SEM)

SEM images in Fig. 4 (A, and B) display various magnifications of the Fe_2O_3-impregnated sample.

As indicated in Fig. 4, the impregnation technique resulted in an increased porosity of clay. This change in appearance may be attributed to alteration in the particle surface charge, resulting from the impregnation and reduction of specific amorphous phases, initially linked to the clay [47]. Additionally, in the treated clay impregnated with Fe_2O_3, various Fe_2O_3 crystals are dispersed on the support surface. It is worth noting that the distribution of Fe_2O_3 particles is not uniform on the surface.

3.1.4. Energy dispersive X-ray (EDX) analysis

To determine its elemental composition, the clay sample was analyzed using energy-dispersive X-ray (EDX) technique. The results are depicted in the EDX image in Fig. 5, while the percentages of elemental composition in the clay are summarized in Table 1.

The chemical analysis of the clay indicates that the constituent elements include oxygen (O), silicon (Si), aluminum (Al), sodium (Na), magnesium (Mg), chlorine (Cl), potassium (K), calcium (Ca), and iron (Fe).

According to the energy dispersive X-ray (EDX) results (Fig. 5 and Table 1), the main constituents of the clay are Oxygen (O), silicon (Si) and aluminum (Al) with percentages of 60.72 %, 17.34 % and 10.66 %, respectively.

The percentages of other metals, including Na, Mg, Cl, K, Ca, and Fe,

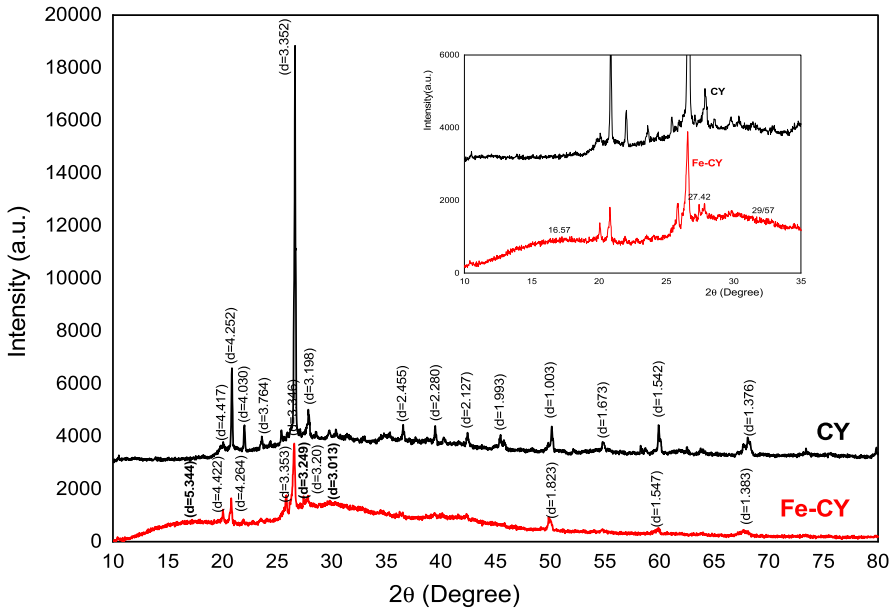

Fig. 2. XRD Diffractogram of treated clay and Fe-CY catalyst.

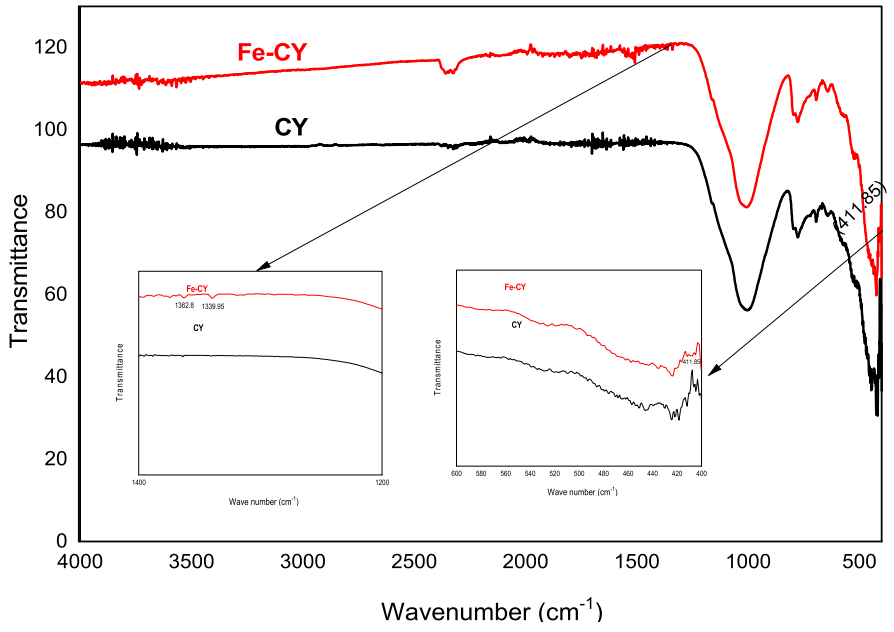

Fig. 3. FTIR spectra of treated clay and Fe-CY catalyst.

are as follows: 5.98 %, 2.89 %, 0.89 %,0.64 %,0.26 %, and 0.62 %. Based on the results obtained and following the investigations conducted by González-Santamaría et al. [48] and Sabbagh et al. [49], the classification of the studied clay as bentonite has been confirmed.

3.1.5. *Specific surface area and porous structure*

The porous structure and specific surface area of the catalyst were assessed using nitrogen gas adsorption–desorption isotherms analyzed via the BET technique. Fig. 6 illustrates a type IV adsorption isotherm, classified according to IUPAC standards, confirming the mesoporous nature of the catalyst. Furthermore, the total pore volume was quantified as 0.215 cm^3/g, with a specific surface area of 23.696 m^2/g. The average pore diameter, calculated as 5.409 nm, corroborates the prevalence of mesopores. Detailed texture properties are summarized in Table 2.

3.2. *Photo-Fenton degradation of MB dye*

Prior to investigating the factors affecting MB discoloration, a batch of tests was conducted to evaluate the catalytic activity of Fe-CY catalyst. The discoloration of MB dye was compared across various systems. Fig. 7 shows that low discoloration occurred in the absence of catalyst and in the presence of sunlight. A small enhancement in dye degradation was noted when sunlight was present alongside H_2O_2 molecules. Conversely, the presence of both catalyst and H_2O_2in dark improved the percentage of pollutant degradation. This improvement is possibly attributed to MB adsorption onto the catalyst and the increased number of free •OH radicals, generated during the adsorption of H_2O_2 molecules onto the catalyst surface. The CY/H_2O_2/solar system exhibits acceptable catalytic performance with MB degradation rate of 80 % over 180 min. After Fe loading, catalytic activity can be significantly

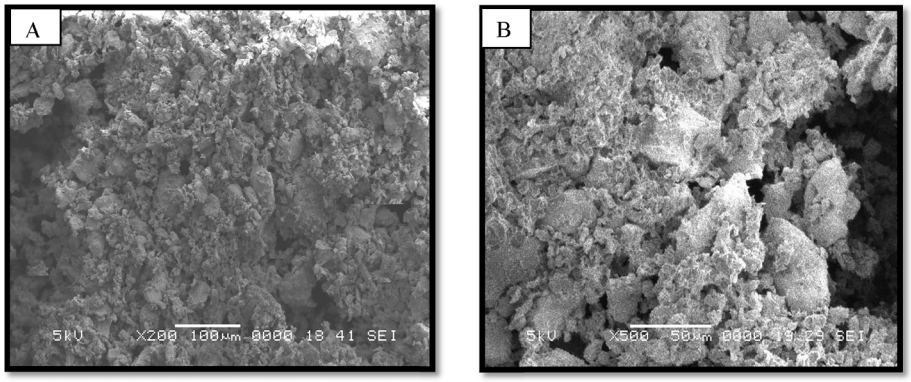

Fig. 4. SEM images of Fe-CY catalyst with various magnifications.

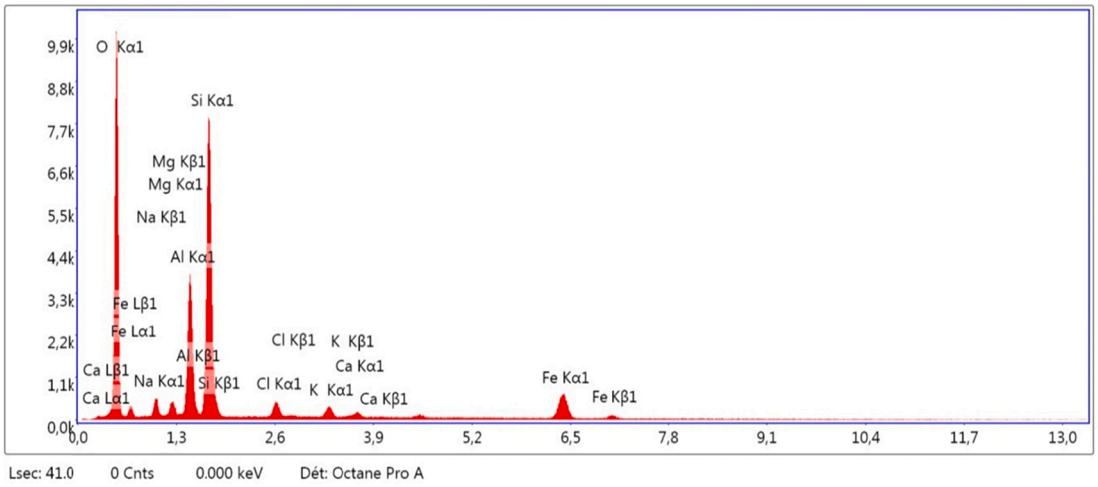

Fig. 5. EDX spectra of the studied sample (CY).

Table 1
EDX analysis results of elemental compositions for treated clay (CY).

Element	Weight %	Atomic %
O	60.72	72.35
Na	5.98	4.96
Mg	2.89	2.27
Al	10.66	7.53
Si	17.34	11.77
Cl	0.89	0.48
K	0.64	0.31
Ca	0.26	0.12
Fe	0.62	0.21

improved. As illustrated in Fig. 5, the presence of sunlight, catalyst, and oxidizing agent stimulates the production of •OH free radicals, which are accountable for the degradation of MB. Consequently, a slight enhancement in discoloration was attained under these conditions, and the Fe-clay/H_2O_2/sunlight combination yielded the best degradation rate of 95.98 % during 180 min.

Eqs. (4) (11) show the mechanism of the Fenton and photo-Fenton process, respectively [48–50].

$$Fe^{3+}sites + H_2O_2 \rightarrow Fe^{3+}sites H_2O_2 \quad (4)$$

$$Fe^{3+}sites + H_2O_2 \rightarrow Fe^{2+}sites + \bullet HO_2 + H^+ \quad (5)$$

$$Fe^{3+}sites + \bullet HO_2 \rightarrow Fe^{2+}sites + O_2 + H^+ \quad (6)$$

$$Fe^{2+}sites + H_2O_2 \rightarrow Fe^{3+}sites + \bullet OH + OH^- \quad (7)$$

$$H_2O_2 + h\gamma \rightarrow 2\bullet OH \quad (8)$$

$$\text{MB Dye} + \bullet OH \rightarrow H_2O + CO_2 + \text{degraded products} \quad (9)$$

In order to increase the conversion of Fe^{3+} to Fe^{2+} ions and favor the generation of hydroxyl radicals (•OH), Fe^{2+} ions were also created from $Fe(OH)^{2+}$ in the presence of light [50].

$$Fe(OH)^{2+} + h\gamma \rightarrow Fe^{2+}\ sites + \bullet OH \quad (10)$$

Or

$$Fe^{3+} + H_2O + h\gamma \rightarrow Fe^{2+} + \bullet OH + H^+ \quad (11)$$

3.3. Solar photo degradation of MB dye

Different factors, including catalyst dosage, H_2O_2 amount, pH, and initial MB concentration were analyzed to investigate the catalytic properties of the produced catalyst, in the photo-Fenton oxidation reaction of MB under direct sunlight.

3.3.1. pH effect

In the pH range of 1.5–10 with H_2O_2 concentration of 5 mmol/L, catalyst dosage of 0.2 g/L, and initial MB concentration of 20 mg/L, the influence of initial pH value was examined on the discoloration of MB in the presence of sunlight.

The results in Fig. 8 indicate that the most efficient pH for the

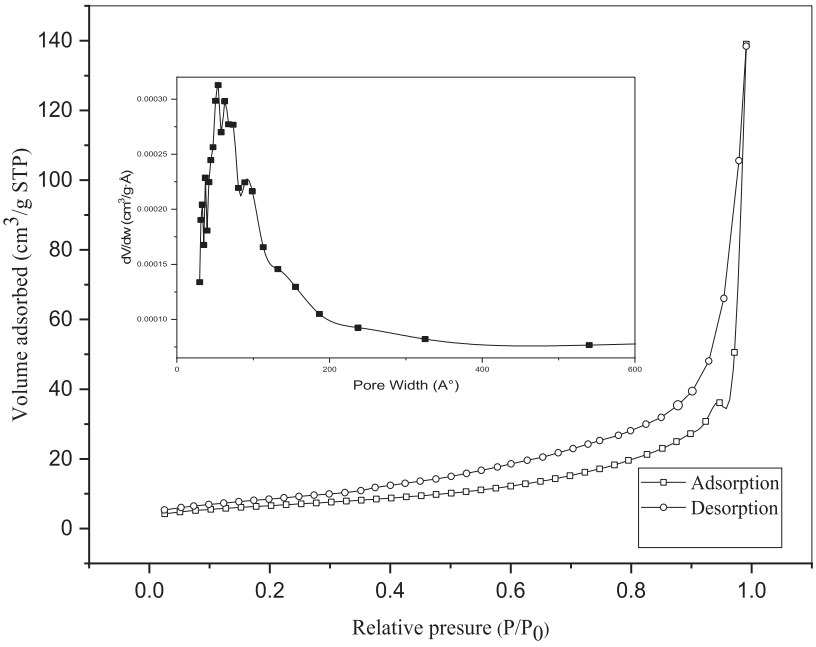

Fig. 6. N_2 adsorption–desorption isotherms and pore size distribution curves of Fe –CY catalyst.

Table 2
Texture properties determined by N_2 adsorption–desorption for (Fe-CY) catalyst.

Method	S_{BET} (m^2/g)	Pore Volume (cm^3/g)	Pore Size (nm)
BET	23.696	0.215	5.409

discoloration of MB was achieved at pH 2.5, resulting in 99.5 % discoloration rate over a duration of 180 min. The decomposition rate of MB exhibited an increase upon increasing pH from 1.5 to 2.5. However, the decomposition performance decreased as pH increased beyond 2.5. The decrease in dye decomposition below pH values of 2.5 may be attributed to stabilization of H_2O_2, through the formation of $H_3O_2^+$ compounds (oxonium ions) caused by protonation of hydrogen peroxide with H^+, thereby converting hydroxyl radicals into water molecules. Additionally, this may lead to the formation of FeO_2^+ as an inactive ion, or additional protons (H^+) may trap •OH radicals as per Eqs. (12) and (13), respectively. On the contrary, the decomposition of hydrogen peroxide results in the generation of water and oxygen and the formation of less active ferryl ions (FeO_2^+), leading to a reduction in MB degradation efficiency at higher pH values, as shown in Eqs. (14) and (15) [51]. Therefore, the most efficient pH value is 2.5.

$$H^+ + H_2O_2 \rightarrow H_3O^{2+} \quad (12)$$

$$H^+ + e^- + \bullet OH \rightarrow H_2O \quad (13)$$

$$H_2O_2 + Fe^{2+} \rightarrow H_2O + FeO^{2+} \quad (14)$$

$$2H_2O_2 \rightarrow O_2 + 2H_2O \quad (15)$$

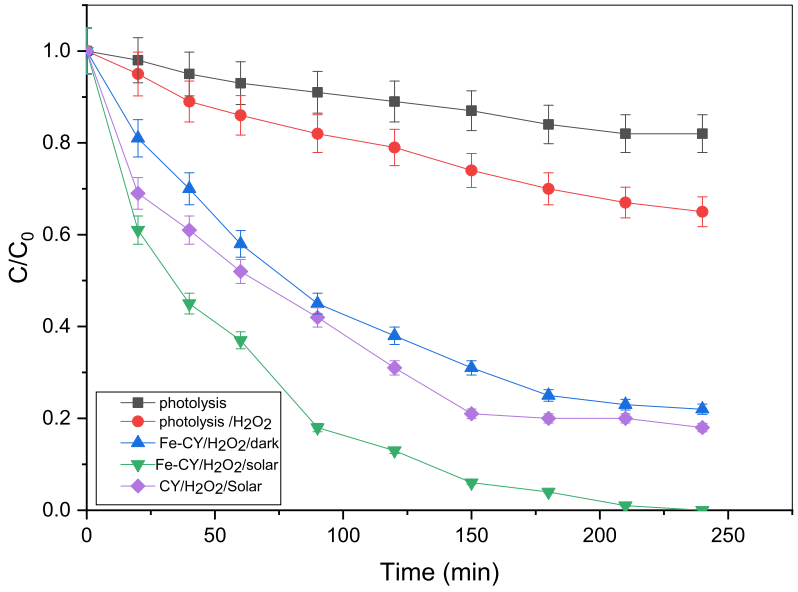

Fig. 7. Comparison of MB degradation under different reaction systems: (a)Photolysis; (b) photolysis/H_2O_2; (c) Fe-CY/H_2O_2/dark; (d)Fe-CY/H_2O_2/solar; (e) CY/H_2O_2/solar.

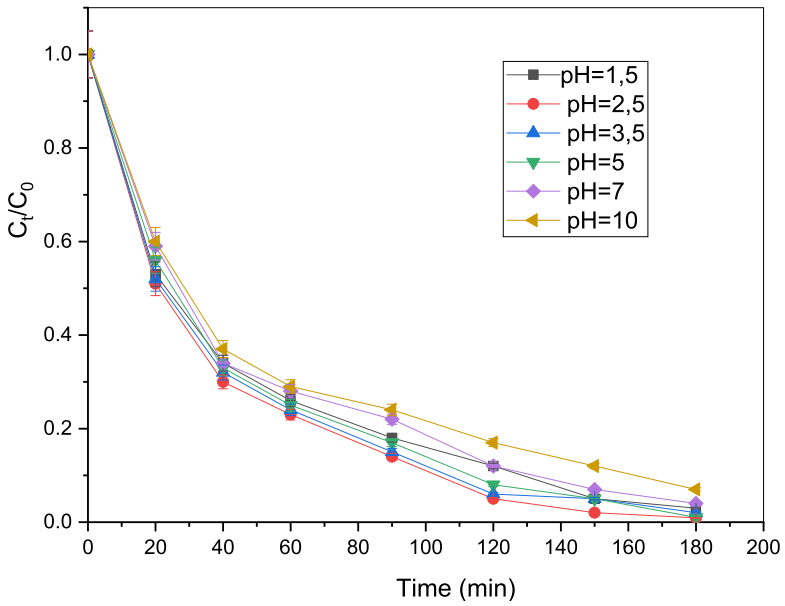

Fig. 8. The pH effect on the degradation of MB under sunlight, reaction conditions: ([MB] 20 mg/L, [H_2O_2] 5 mM, catalyst dose 0.2 g/L and T 28 ± 2°C).

3.3.2. Oxidant amount effect

The influence of varying H_2O_2 doses on MB decomposition was examined by introducing different volumes of H_2O_2 (3, 5, and 8 mmol/L) under specific conditions: a catalyst dose of 0.2 g/L, a dye concentration of 20 mg/L, solution pH set at 2.5, and a temperature maintained at 28 ± 2°C. The results are depicted in Fig. 9.

Without H_2O_2, no significant color removal was observed. However, adjusting the initial concentration of H_2O_2 from 3 to 8 mmol/L revealed its impact on the decomposition of MB. The findings in Fig. 9 indicate that the rate of MB removal increased with time as H_2O_2 dose was increased from 3-8 mmol/L. Thus, the quantity of •OH radicals, accountable for the dye disintegration, increases proportionally with H_2O_2 concentration in solution. The optimal concentration of H_2O_2 for the photo-Fenton process was found to be 8 mmol/L, resulting in a catalytic degradation rate of 99.5 % for MB.

3.3.3. Catalyst dosage effect

The effect of catalyst dosage on MB discoloration was examined by varying the catalyst mass from 0.1 to 0.4 g/L. The results are depicted in Fig. 10. The MB discoloration was significantly related to the catalyst dose. It was observed that varying catalyst masses cause the C_t/C_0 ratio to decline more quickly over time, this can be explained by the fact that more reactive sites become available on the catalyst surface, as catalyst dosage is increased, which allows for the production of more reactive radicals. Another explanation could be that a higher dose of catalyst provides a larger surface area, which leads to an increased interaction between the organic dye and reactive species formed on the catalyst surface, thus enhancing the MB removal efficiency. Furthermore, as the reaction between ferrous ions and oxidizing agent H_2O_2 occurs on the catalyst surface, the number of active sites becomes crucial in determining the efficiency of dye degradation and overall catalytic activity. Our findings indicate that employing 0.4 g and 0.2 g of catalyst for 180

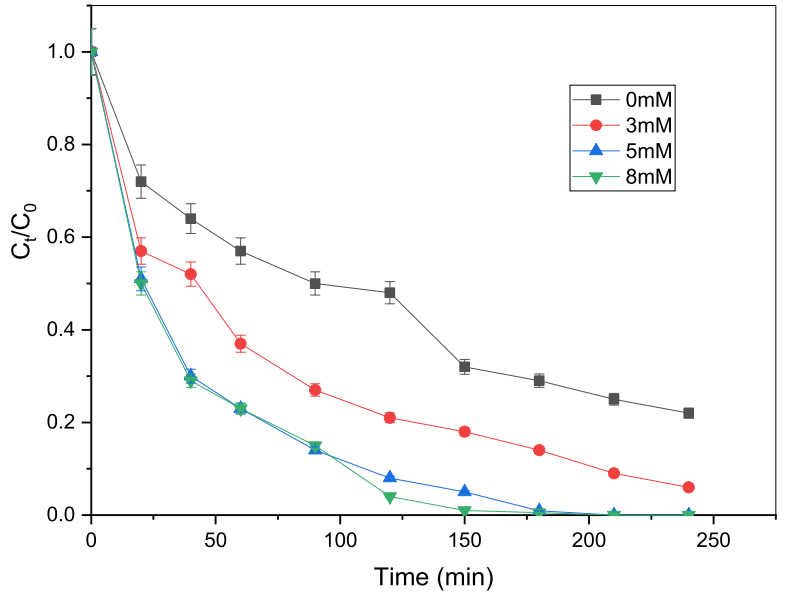

Fig. 9. Effect of hydrogen peroxide concentration on MB degradation under sunlight. Reaction conditions: [MB] 20 mg/L, catalyst dose 0.2 g/L, pH 2.5, and T 28 ± 2°C.

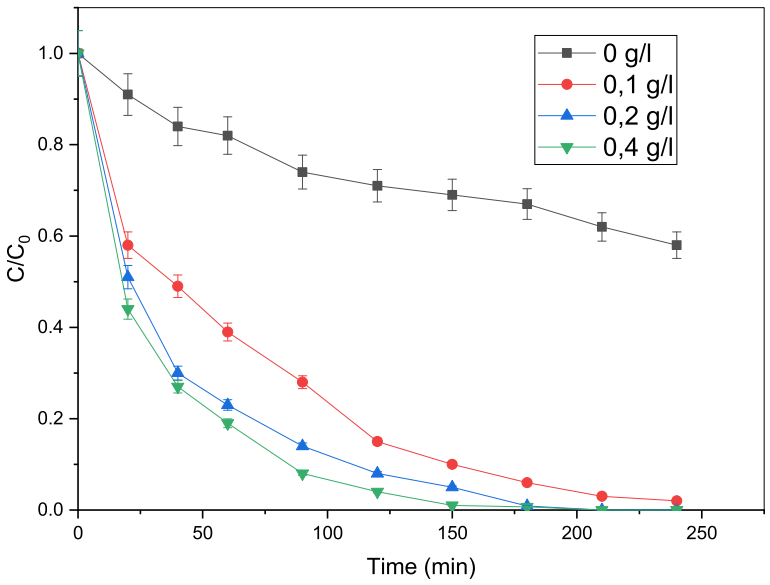

Fig. 10. Effect of catalyst dose on the degradation of MB under sunlight. Reaction conditions: [MB] 20 mg/l, [H_2O_2] 8 mM, catalyst dose 0.2 g/l, pH 2.5, and T 28 ± 2°C.

min resulted in the highest rate of MB degradation, with a slight advantage observed in the case of 0.4 g. For considerations of both efficiency and cost, the use of 0.2 g of catalyst for subsequent reactions was chosen.

3.3.4. Initial MB concentration effect

To investigate the impact of the initial pollutant concentration on the photocatalytic process, various concentrations of MB solution (ranging from 10 to 80 mg/L) were tested, as shown in Fig. 11.

The degradation efficiency decreased as the concentration of initial MB increased. The most significant MB degradation occurred at a concentration of 10 mg/L after 180 min. Therefore, the Fe-CY photocatalytic process operates more effectively at lower MB concentrations. This may be attributed to high solar penetration efficiency in MB solution at low concentrations, or to tendency of molecular dye to adhere to the catalyst surface, thus more easily occupying the active sites.

3.4. MB degradation via microwave-assisted photocatalysis

The Fe-CY catalyst was investigated for its effect on the degradation of MB at microwave power levels of 200, 350, and 500 W.

The results depicted in Fig. 12 display a clear correlation between microwave power and degradation. C_t/C_0 ratio gradually decreases over time, regardless of the presence or absence of catalyst. However, the influence of the catalyst is more evident in MB decomposition at varying microwave power levels. The catalyst enhances the reaction, yielding optimal outcomes at a power level of 500 W, compared to 200 W. The maximum level of degradation is 95.5 %, and it takes 8 min to reach this value. This notable outcome is attributed to synergistic interaction between Fenton and microwaves. This interaction generates additional •OH radicals, which are largely responsible for the breakdown of MB dye. Consequently, the following equations: (Eqs. (16) and (17)) can be used to elucidate the production of •OH and regeneration of Fe^{2+} from Fe^{3+}, through microwave reduction in this system.

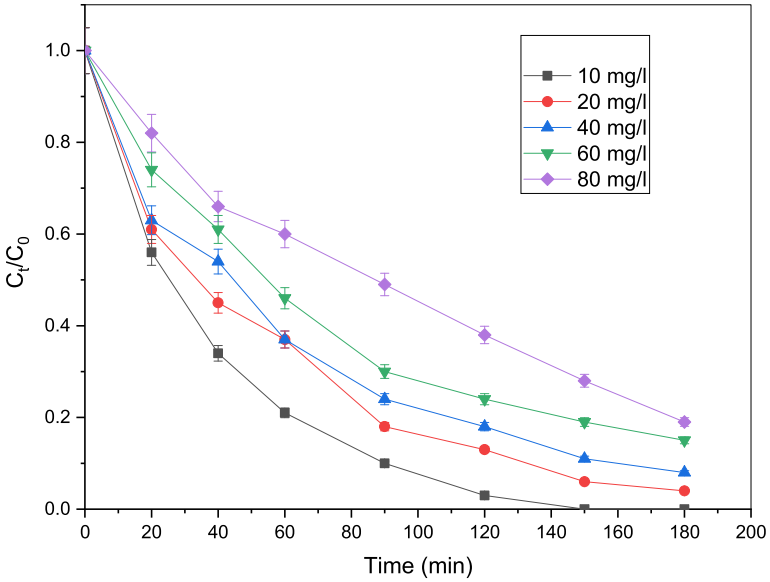

Fig. 11. Effect of initial MB concentration on MB degradation. Reaction conditions: [H_2O_2] 8 mM, catalyst dose 0.2 g/L, pH 2.5, T 28 ± 2°C.

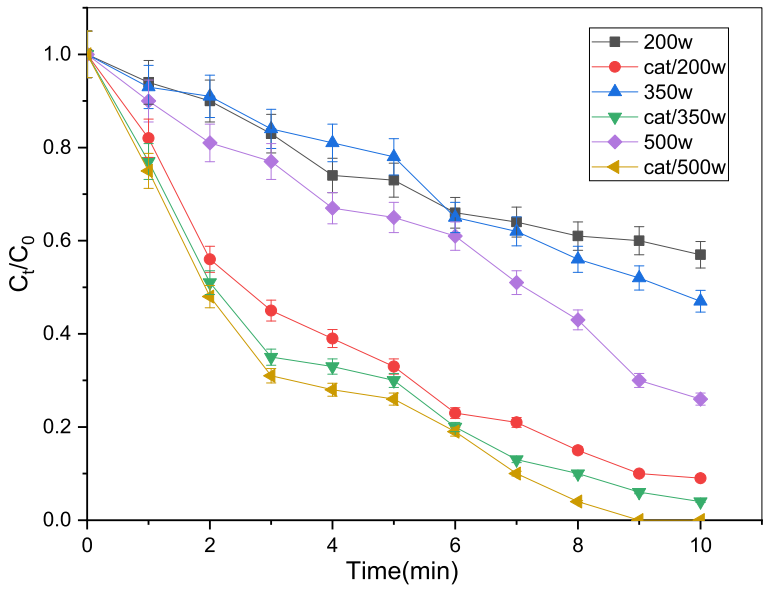

Fig. 12. Kinetic curves for the degradation of MB solution, resulting from photocatalytic reaction in the presence and absence of catalysts under a) 200, b) 250, and c) 500 w microwave oven power.

$$Fe^{2+} + H_2O_2 + \text{microwave} \rightarrow Fe^{3+} + \bullet OH + OH \quad (16)$$

$$Fe(OH)^{2+} + \text{microwave} \rightarrow Fe^{3+} + \bullet OH \quad (17)$$

As a result, the microwave-Fenton process improved the rate of MB discoloration and reduced the reaction time.

3.5. Kinetic study of MB dye degradation reaction

3.5.1. Catalyst kinetics with different systems

The most common model for describing the kinetics of heterogeneous photocatalysis is Langmuir Hinshelwood equation model. The simplification of this equation leads to the establishment of a first-order pseudo-kinetic equation.

$$\ln\frac{C_t}{C_0} = \quad kt \quad (18)$$

Where: C_0 and C_t are the initial concentration and final concentration after photocatalytic degradation process, respectively, at time t. The results from Fig. 13 indicated that among the five processes, photo-Fenton was the most effective, with a rate coefficient value of 0.0176, which is higher than that of the other systems; the photocatalytic degradation follows Langmuir-Hinshelwood model expressed in pseudo-first order, as evidenced by R^2 values, demonstrating acceptable linearity.

The kinetic parameters of photocatalytic MB discoloration, whose $t_{1/2}$ value is calculated using 0.693/k are reported in Table 3.

3.5.2. Catalyst kinetics with different microwave powers

The results presented in Table 4 and Fig. 14 demonstrate that all

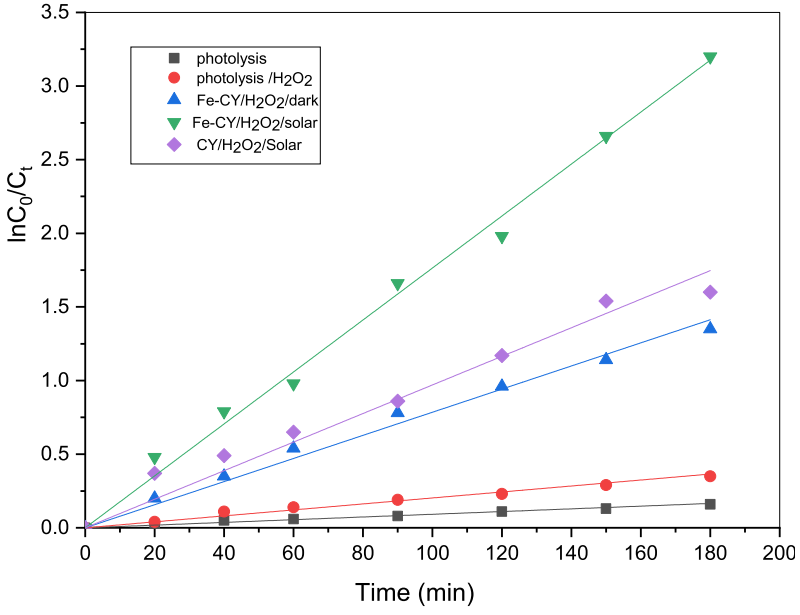

Fig. 13. Pseudo-first order kinetic plot for MB degradation in different reaction systems.

Table 3
Effect of different systems on the simultaneous MB elimination.

System	K_a	$t_{1/2}$ (min)	R^2
Photolysis	0.0009	770.16	0.9836
Photolysis /H_2O_2	0.0020	346.57	0.9829
Fe-CY/H_2O_2/dark	0.0078	88.86	0.9870
Fe-CY/H_2O_2/solar	0.0176	39.38	0.9935
CY/H_2O_2/Solar	0.0097	71.45	0.9677

solutions exhibit first-order kinetics for the degradation reaction of MB, with varying microwave powers. As the power for both systems increases, the value of rate constant K_a also increases.

K_a is notably higher in the presence of Fe-CY catalyst, when compared to the absence of catalyst. Additionally, the K_a rate constants for the microwave-Fenton process are significantly higher, when compared to those of solar-Fenton.

Due to varying experimental conditions, direct comparison of the observed MB degradation rates in this study with those previously reported in the literature is challenging. Nevertheless, Table 5 illustrates that the Fe-CY catalyst used in this study exhibited superior MB removal efficiency, compared to other catalysts. The comparison shows that the Fe-CY catalyst has great potential for photocatalytic degradation of MB in wastewater.

3.6. Catalyst system stability

From both industrial and environmental perspectives, the reusability of catalyst is a crucial aspect.

The reuse tests were conducted to assess the catalytic activity of Fe-CY over subsequent experiments and determine the feasibility of using the catalyst again. It should be noted, as previously mentioned, that after each test, the catalyst is separated from its suspensions by simple centrifugation, washed and dried with excess distilled water and acetone at 110 °C, respectively, then reused. According to the results summarized in Fig. 15, it is evident that the Fe-CY catalyst, used in MB degradation in sunlight, exhibited a minor reduction in efficiency of 1.73 %, 3.8 % and 7.4 %, during the initial three rounds of testing due to catalyst surface deactivation. This outcome emphasizes the outstanding stability and user-friendliness of catalyst.

3.7. Degradation mechanism

A potential mechanism for the Fe-CY heterogeneous catalyst, as illustrated in Fig. 16, was proposed to elucidate its role in the discoloration and mineralization of MB. Our findings indicate that, under complete darkness, MB was adsorbed onto the Fe-CY catalyst surface. Subsequently, under sunlight or microwave irradiation, photo-reduction

Table 5
Comparison of photocatalytic performance in MB dye degradation by various catalysts under different conditions.

Catalyst	Catalyst quantity	Light source used	Degradation %	References
Fe/Al_2O_3-MCM-41	1 g/l	sunlight	100	[52]
Ag@AgCl-TiO_2/sepiolite	0.15 g/l	Visible light	82.72	[53]
Fe_3O_4/Zeolite A	0.6 g/l	UV Lamp (6w)	100	[54]
Fe_3O_4/$Ag_6Si_2O_7$	0.1 g/l	Visible light	98	[55]
Ag-K-T	0.5 g/l	Visible light	94.8	[56]
Iron–rich clay	0.02 g	Visible light	94	[57]
Zn/CeO_2@BC	0.2 g/l	Sun light	98.24	[58]
Fe-CY	0.2 g/l	Sun light	99.5	This work
Fe-CY	0.2 g/l	Microwave irradiation	95.5	This work

Table 4
Kinetic constants for first-order reactions for different microwave powers.

	Power = 200 W			Power = 350 W			Power = 500 W		
System	K_a	$t_{1/2}$	R^2	K_a	$t_{1/2}$	R^2	K_a	$t_{1/2}$	R^2
Without catalyst	0.059	11.74	0.99	0.068	10.19	0.98	0.094	7.37	0.99
Fe-CY	0.238	2.91	0.99	0.29	2.32	0.99	0.33	2.10	0.97

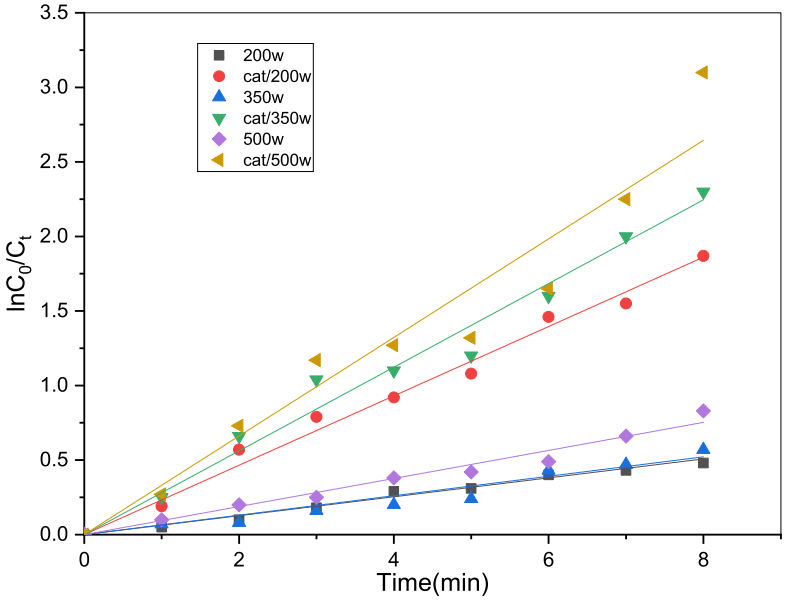

Fig. 14. Pseudo-first order kinetic plot for MB degradation at different microwave powers.

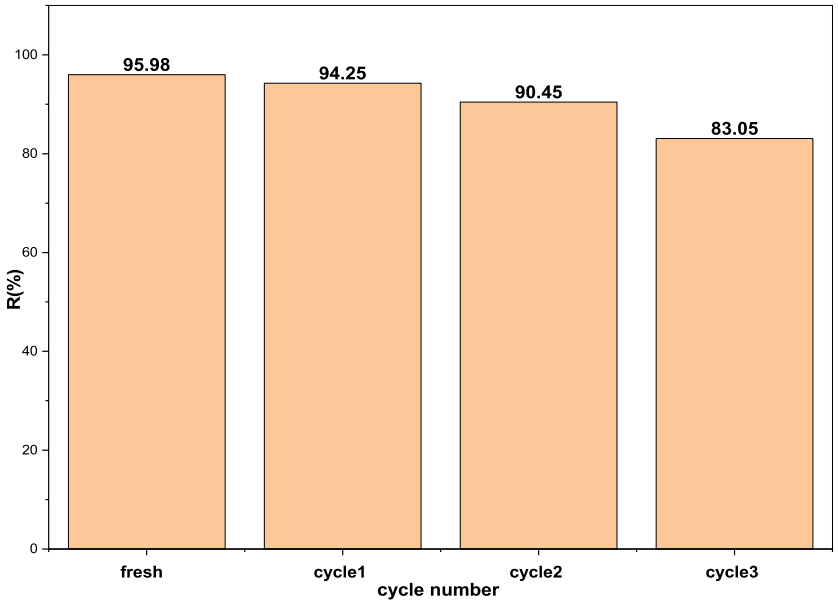

Fig. 15. Percentage of MB degradation with Fe-CY on photo-Fenton process under sunlight at 180 min after 3 cycles.

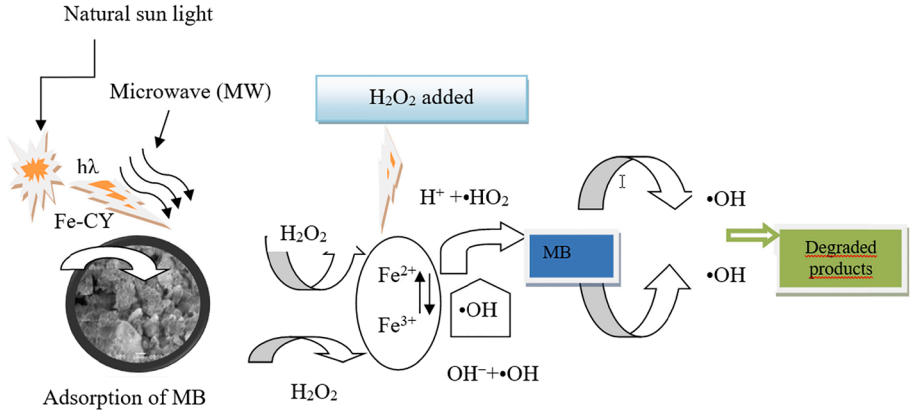

Fig. 16. Mechanism of heterogeneous photo-Fenton process.

of Fe^{3+} to Fe^{2+} on the Fe-CY surface initiated the processes. The cycle of Fe^{3+}/Fe^{2+} was completed when Fe^{2+} produced by the reaction with H_2O_2 reacted with •OH radicals [59]. •OH radicals attacked MB molecules adsorbed onto the surface of Fe-CY catalyst, producing reaction intermediates. The degradation of chemical intermediates ultimately yields CO_2, H_2O, and mineralization products.

4. Conclusion

In this investigation, the catalytic characteristics of supported Fe-CY catalyst in the photo-Fenton process for degrading MB dye was examined using two varying irradiation sources (microwave or solar) along with varying concentrations of initial H_2O_2, catalyst dose, pH and light irradiation conditions. The optimum photo-Fenton reaction conditions for eliminating MB were identified as 8 mM H_2O_2, 0.2 g/L Fe-CY and 10 mg/L MB at an initial pH of 2.5. Under these conditions, the MB discoloration efficiency was 99.5 % and 95.5 % during 180 and 8 min of sunlight and microwave irradiation, respectively. According to the kinetic study, the MB degradation in aqueous solution, using the photo-Fenton process, and in the presence of heterogeneous catalyst, follows the pseudo-first order. In summary, our results demonstrate that both the microwave-Fenton and solar-Fenton processes are viable methods for the degradation and mineralization of MB dye. The simplicity and cost-effectiveness of the solar-Fenton method make it a practical choice, while the microwave-Fenton process exhibits faster dye degradation. Additionally, Fe-CY emerges as a highly effective heterogeneous catalyst for MB discoloration due to its chemical stability, excellent catalytic activity, non-toxic nature and ease of recyclability.

CRediT authorship contribution statement

Amel Lounnas: Writing – original draft, Methodology, Investigation, Formal analysis. **Abdelhak Moumen:** Visualization, Validation, Supervision, Methodology, Investigation, Funding acquisition, Formal analysis, Data curation, Conceptualization. **Emna Zouaoui:** Visualization, Formal analysis. **Youghourta Belhocine:** Writing – original draft, Supervision. **Chafia Sobhi:** Validation, Methodology, Formal analysis. **Seyfeddine Rahali:** Writing – original draft, Software. **Najoua Sbei:** Writing – original draft, Formal analysis, Conceptualization.

Declaration of competing interest

The authors declare that they have no known competing financial interests or personal relationships that could have appeared to influence the work reported in this paper.

Data availability

No data was used for the research described in the article.

References

[1] S. Biswas, T.U. Rashid, T. Debnath, P. Haque, M.M. Rahman, Application of chitosan-clay biocomposite beads for removal of heavy metal and dye from industrial effluent, J. Compos. Sci. 4 (2020) 16.

[2] H. Solayman, M.A. Hossen, A. Abd Aziz, N.Y. Yahya, L.K. Hon, S.L. Ching, M. U. Monir, K.-D. Zoh, Performance evaluation of dye wastewater treatment technologies: a review, J. Environ Chem. Eng. 11 (2023) 109610.

[3] M. Shabir, M. Yasin, M. Hussain, I. Shafiq, P. Akhter, A.-S. Nizami, B.-H. Jeon, Y.-K. Park, A review on recent advances in the treatment of dye-polluted wastewater, J. Ind. Eng. Chem. 112 (2022) 1–19.

[4] S. Thomas, S. Nair, K. Rajesh, R. Nath, Highly efficient recyclable copper (I) chloride complex catalysts having photo-Fenton activity for methylene blue degradation by sunlight, Inorg. Chem. Comm. 153 (2023) 110745.

[5] A. Moumen, Y. Belhocine, F. Mechati, M. Karout, D. Charime, W. Boultif, Z. Hattab, Spectral, isotherm, kinetic, and thermodynamic studies of malachite green dye adsorption from aqueous solutions onto low-cost treated kaolin, Phys. Chem. Res. 12 (2024) 47–60.

[6] B.F. Far, M.R. Naimi-Jamal, M. Jahanbakhshi, M. Alian, D.R. Jahromi, Decontamination of Congo red dye from aqueous solution using nanoclay/chitosan-graft-gelatin nanocomposite hydrogel, J. Mol. Liq. 395 (2023) 123839.

[7] A. Moumen, Y. Belhocine, N. Sbei, S. Rahali, F.A.M. Ali, F. Mechati, F. Hamdaoui, M. Seydou, Removal of malachite green dye from aqueous Solution by catalytic wet oxidation technique using Ni/kaolin as catalyst, Molecules 27 (2022) 7528.

[8] F.Z. Gharbi, N. Bougdah, Y. Belhocine, N. Sbei, S. Rahali, M. Damous, M. Seydou, Green and fast extraction of chitin from waste shrimp Shells: characterization and application in the removal of Congo Red Dye, Separations 10 (2023) 599.

[9] S.F. Almojil, J. Ning, A.I. Almohana, Photo-Fenton process for degradation of methylene blue using copper ferrite@sepiolite clay, Inorg. Chem. Commun. 166 (2024) 112623.

[10] N. Hamrouche, C. Djilani, P. Magri, Y. Belhocine, F. Djazi, M. Kezzar, N. Bouzenad, A novel biosorbent from raw pomegranate peel modified with $SnCl_2$/$FeCl_2$ for the adsorption of crystal violet cationic dye: response surface methodology process optimization, thermodynamic, kinetic, isotherm, and recyclability studies, Biomass Conv. Bioref. (2024), https://doi.org/10.1007/s13399-024-05737-5.

[11] K. He, M. Yan, Z. Huang, G. Zeng, A. Chen, T. Huang, H. Li, X. Ren, G. Chen, Fabrication of ploydopamine–kaolin supported Ag nanoparticles as effective catalyst for rapid dye decoloration, Chemosphere 219 (2019) 400–408.

[12] I. Khan, K. Saeed, I. Zekker, B. Zhang, A.H. Hendi, A. Ahmad, S. Ahmad, N. Zada, H. Ahmad, L.A. Shah, T. Shah, Review on methylene blue: its properties, uses, toxicity and photodegradation, Water 14 (2022) 242.

[13] R. Al-Tohamy, S.S. Ali, F. Li, K.M. Okasha, Y.-A.-G. Mahmoud, T. Elsamahy, H. Jiao, Y. Fu, J. Sun, A critical review on the treatment of dye-containing wastewater: ecotoxicological and health concerns of textile dyes and possible remediation approaches for environmental safety, Ecotoxicol. Environ. Saf. 231 (2022) 113160.

[14] M. Fayazi, M.A. Taher, D. Afzali, A. Mostafavi, Enhanced Fenton-like degradation of methylene blue by magnetically activated carbon/hydrogen peroxide with hydroxylamine as Fenton enhancer, J. Mol. Liq. 216 (2016) 781–787.

[15] O.G. Júnior, M.G.B. Santos, A.B. Nossol, M.C.V. Starling, A.G. Trovó, Decontamination and toxicity removal of an industrial effluent containing pesticides via multistage treatment: coagulation-flocculation-settling and photo-Fenton process, Process. Saf. Environ. Prot. 147 (2021) 674–683.

[16] A. Mahto, K. Aruchamy, R. Meena, M. Kamali, S.K. Nataraj, T.M. Aminabhavi, Forward osmosis for industrial effluents treatment–sustainability considerations, Sep. Purif. Technol. 254 (2021) 117568.

[17] T.G. Kebede, A.A. Mengistie, S. Dube, T.T. Nkambule, M.M. Nindi, Study on adsorption of some common metal ions present in industrial effluents by Moringa stenopetala seed powder, J. Environ. Chem. Eng. 6 (2018) 1378–1389.

[18] M.G. Ghoniem, F.A.M. Ali, B.Y. Abdulkhair, M.R.A. Elamin, A.M. Alqahtani, S. Rahali, M.A. Ben Aissa, Highly selective removal of cationic dyes from wastewater by MgO nanorods, Nanomaterials 12 (2022) 1023.

[19] L. Castro, M.L. Blázquez, F. González, J.A. Muñoz, A. Ballester, Biosorption of Zn (II) from industrial effluents using sugar beet pulp and F. vesiculosus: From laboratory tests to a pilot approach, Sci. Total Environ. 598 (2017) 856–866.

[20] S.S. Chandrasekhar, D. Vaishnavi, N. Sahu, S. Sridhar, Design of an integrated membrane bioreactor process for effective and environmentally safe treatment of highly complex coffee industrial effluent, J. Water Process Eng. 37 (2020) 101436.

[21] V. Katheresan, J. Kansedo, S.Y. Lau, Efficiency of various recent wastewater dye removal methods: a review, J. Environ. Chem. Eng. 6 (2018) 4676–4697.

[22] M.A. Oturan, J.-J. Aaron, Advanced oxidation processes in water/wastewater treatment: principles and applications. A review, Crit. Rev. Environ. Sci. Technol. 44 (2014) 2577–2641.

[23] H. Godini, A. Sheikhmohammadi, L. Abbaspour, R. Heydari, G.S. Khorramabadi, M. Sardar, Z. Mahmoudi, Energy consumption and photochemical degradation of Imipenem/Cilastatin antibiotic by process of UVC/Fe^{2+}/H_2O_2 through response surface methodology, Optik 182 (2019) 1194–1203.

[24] A. Saravanan, V.C. Deivayanai, P.S. Kumar, G. Rangasamy, R.V. Hemavathy, T. Harshana, N. Gayathri, K. Alagumalai, A detailed review on advanced oxidation process in treatment of wastewater: mechanism, challenges and future outlook, Chemosphere 308 (2022) 136524.

[25] S. Minz, S. Gara, R. Gupta, Effect of operating parameters, reaction kinetics and comparative assessment of fluidized-bed fenton Oxidation of 4-Nitrophenol, Iran. J. Chem. Chem. Eng. 40 (2021) 539–550.

[26] A. Carrillo, J. Carriazo, Cu and Co oxides supported on halloysite for the total oxidation of toluene, Appl. Catal. B Environ. 164 (2015) 443–452.

[27] J. Zhu, X. Zhu, F. Cheng, P. Li, F. Wang, Y. Xiao, W. Xiong, Preparing copper doped carbon nitride from melamine templated crystalline copper chloride for Fenton-like catalysis, Appl. Catal. B 256 (2019) 117830.

[28] S. Eslaminejad, R. Rahimi, M. Fayazi, Sepiolite-metal organic framework-iron oxide catalyst for degradation of Rhodamine B using Fenton-like process, J. Taiwan Inst. Chem. Eng. 152 (2023) 105181.

[29] J.T. Hernández-Oloño, A. Infantes-Molina, D. Vargas-Hernández, D.G. Domínguez-Talamantes, E. Rodríguez-Castellón, J.R. Herrera-Urbina, J.C. Tánori-Córdova, A novel heterogeneous photo-Fenton Fe/Al_2O_3 catalyst for dye degradation, J. Photochem. Photobiol. A 421 (2021) 113529.

[30] U. Vengatakrishnan, K. Subramanian, V. Rajapandi, D.N. Raman, Effect of ultraviolet and solar radiation on photocatalytic dye (Black-E and Congo red) degradation using copper oxide nanostructure particles, Iran. J. Mater. Sci. Eng. 18 (2021) 1–12.

[31] V. Kavitha, K. Palanivelu, Degradation of phenol and trichlorophenol by heterogeneous photo-Fenton process using Granular Ferric Hydroxide®: comparison with homogeneous system, Int. J. Environ. Sci. Technol. 13 (2016) 927–936.

[32] S. Li, G. Zhang, W. Zhang, H. Zheng, W. Zhu, N. Sun, Y. Zheng, P. Wang, Microwave enhanced Fenton-like process for degradation of perfluorooctanoic acid (PFOA) using Pb-$BiFeO_3$/rGO as heterogeneous catalyst, Chem. Eng. J. 326 (2017) 756–764.

[33] S. Farazmand, M. Fayazi, Single-step solvothermal synthesis of sepiolite-$CoFe_2O_4$ nanocomposite as a highly efficient heterogeneous catalyst for photo Fenton-like reaction, Mater. Chem. Phys. 312 (2024) 128627.

[34] M. Saeed, M. Muneer, N. Akram, A. ul Haq, N. Afzal, M. Hamayun, Synthesis and characterization of silver loaded alumina and evaluation of its photo catalytic activity on photo degradation of methylene blue dye, Chem. Eng. Res. Des. 148 (2019) 218–226.

[35] N.A. Khan, A.H. Khan, P. Tiwari, M. Zubair, M. Naushad, New insights into the integrated application of Fenton-based oxidation processes for the treatment of pharmaceutical wastewater, J. Water Proc. Eng. 44 (2021) 102440.

[36] D. Xie, C. Tang, D. Li, J. Yuan, F. Xu, FeOCl/WS_2 composite as a heterogeneous Fenton catalyst to efficiently degrade acid orange II, Inorg. Chem. Commun. 156 (2023) 111085.

[37] P. Mahamallik, A. Pal, Degradation of textile wastewater by modified photo-Fenton process: application of Co (II) adsorbed surfactant-modified alumina as heterogeneous catalyst, J. Environ. Chem. Eng. 5 (2017) 2886–2893.

[38] H. Alhussain, N.Y. Elamin, L.S. Alqarni, A. Albadri, K.K. Taha, A. Modwi, Purification of RhB dye from aquatic media via CaO-TiO_2@g-C_3N_4 nanocomposite, Inorg. Chem. Commun. 159 (2024) 111785.

[39] S. Mustapha, J. Tijani, M. Ndamitso, S. Abdulkareem, D. Shuaib, A. Mohammed, A. Sumaila, The role of kaolin and kaolin/ZnO nanoadsorbents in adsorption studies for tannery wastewater treatment, Sci. Rep. 10 (2020) 13068.

[40] I. Fatimah, G. Fadillah, I. Yanti, R.-A. Doong, Clay-supported metal oxide nanoparticles in catalytic advanced oxidation processes: a review, Nanomaterials 12 (2022) 825.

[41] K. Saeed, I. Khan, S.Y. Park, TiO_2/amidoxime-modified polyacrylonitrile nanofibers and its application for the photodegradation of methyl blue in aqueous medium, Desalin. Water Treat. 54 (2015) 3146–3151.

[42] A.Q. Alorabi, M.S. Hassan, M.M. Alam, S.A. Zabin, N.I. Alsenani, N.E. Baghdadi, Natural clay as a low-cost adsorbent for crystal violet dye removal and antimicrobial activity, Nanomaterials 11 (2021) 2789.

[43] M. Soleimani, Z.H. Siahpoosh, Ghezeljeh nanoclay as a new natural adsorbent for the removal of copper and mercury ions: Equilibrium, kinetics and thermodynamics studies, Chin. J. Chem. Eng. 23 (2015) 1819–1833.

[44] M. Nazim, A.A.P. Khan, A.M. Asiri, J.H. Kim, Exploring rapid photocatalytic degradation of organic pollutants with porous CuO nanosheets: Synthesis, dye removal, and kinetic studies at room temperature, ACS Omega 6 (2021) 2601–2612.

[45] E. Mekatel, M. Trari, D. Nibou, I. Sebai, S. Amorkrane, Preparation and characterization of α-Fe_2O_3 supported clay as a novel photocatalyst for hydrogen evolution, Int. J. Hydrogen Energy 44 (2019) 10309–10315.

[46] S. Benkacem, K. Boudeghdegh, F. Zehani, M. Hamidouche, Y. Belhocine, Preparation, microstructure studies and mechanical Properties of glazes ceramic sanitary ware based on kaolin, Sci. Sinter. 53 (2021) 209–221.

[47] H. Hassan, B.H. Hameed, Fe-clay as effective heterogeneous Fenton catalyst for the decolorization of Reactive Blue 4, Chem. Eng. J. 171 (2011) 912–918.

[48] D.E. González-Santamaría, A. Justel, R. Fernández, A.I. Ruiz, A. Stavropoulou, J. D. Rodríguez-Blanco, J. Cuevas, SEM-EDX study of bentonite alteration under the influence of cement alkaline solutions, Appl. Clay Sci. 212 (2021) 106223.

[49] F. Sabbagh, N.M. Khatir, A.K. Karim, A. Omidvar, Z. Nazari, R. Jaberi, Mechanical properties and swelling behavior of acrylamide hydrogels using montmorillonite and kaolinite as clays, J. Environ. Treat. Tech. 7 (2019) 211–219.

[50] Y. Ahmed, Z. Yaakob, P. Akhtar, Degradation and mineralization of methylene blue using a heterogeneous photo-Fenton catalyst under visible and solar light irradiation, Catal, Sci. Technol. 6 (2016) 1222–1232.

[51] M. Dinarvand, M. Sohrabi, S.J. Royaee, V. Zeynali, Degradation of phenol by heterogeneous Fenton process in an impinging streams reactor with catalyst bed, Asia-Pac. J. Chem. Eng. 12 (2017) 631–639.
[52] A.C. Pradhan, K.M. Parida, Facile synthesis of mesoporous composite Fe/Al_2O_3–MCM-41: an efficient adsorbent/catalyst for swift removal of methylene blue and mixed dyes, J. Mater. Chem. 22 (2012) 7567–7579.
[53] S. Liu, D. Zhu, J. Zhu, Q. Yang, H. Wu, Preparation of Ag@AgCl-doped TiO_2/sepiolite and its photocatalytic mechanism under visible light, J. Environ. Sci. 60 (2017) 43–52.
[54] H.G. Quynh, H. Van Thanh, N.T.T. Phuong, N.P.T. Duy, L.H. Hung, N. Van Dung, N.T.H. Duong, N.Q. Long, Rapid removal of methylene blue by a heterogeneous photo-Fenton process using economical and simple-synthesized magnetite–zeolite composite, Environ. Technol. Innov. 31 (2023) 103155–103168.
[55] H. Chen, N. Chen, Y. Gao, C. Feng, Photocatalytic degradation of methylene blue by magnetically recoverable Fe_3O_4/$Ag_6Si_2O_7$ under simulated visible light, Powder Technol. 326 (2018) 247–254.
[56] S. Sharma, A. Devi, K.G. Bhattacharyya, Photocatalytic degradation of methylene blue in aqueous solution with silver-kaolinite-titania nanocomposite under visible light irradiation, J. Nanostruct. 12 (2022) 426–445.
[57] B.M. Zimmermann, E.C. Peres, G.L. Dotto, E.L. Foletto, Decolorization and degradation of methylene blue by photo-Fenton reaction under visible light using an iron-rich clay as catalyst: CCD-RSM design and LC-MS technique, REGET 24 (2020) 27.
[58] A.K. Dey, S.R. Mishra, M. Ahmaruzzaman, Solar light–based advanced oxidation processes for degradation of methylene blue dye using novel Zn-modified CeO_2@biochar, Environ. Sci. Pollut. Res. 30 (2023) 53887–53903.
[59] H.B. Hadjltaief, M.B. Zina, M.E. Galvez, P. Da Costa, Photo-Fenton oxidation of phenol over a Cu-doped Fe-pillared clay, C. R. Chim. 18 (2015) 1161–1169.